Control Theory Tech, Vol. 17, No. 3, pp. 201–215, August 2019

Control Theory and Technology

http://link.springer.com/journal/11768

Parallel loop recovery with quiescent compensation for high performance feedback control of systems with imperfect actuators

Y. V. O'BRIEN†, J. F. O'BRIEN

Department of Electrical and Computer Engineering, University of Wyoming, Laramie, WY 82073, U.S.A.

Received 23 February 2018; revised 29 September 2018; accepted 8 October 2018

Abstract

Actuator limits and imperfections introduce multiple nonlinearities in a feedback loop. While standard mild-feedback systems (e.g., PID) are intrinsically robust to such nonlinearities, the stability of large feedback systems is threatened. This eliminates from consideration the usage of imperfect actuators in large feedback applications and available disturbance rejection as a result is not realized. The implementation of multiple-path nonlinear dynamic compensation (NDC), however, allows the combination of large feedback and imperfect actuation and is the focus of this work. As nonlinearities due to actuator imperfection are often difficult to model, the stability of the NDC systems is assessed using multivariable absolute stability analysis. The features of a parallel loop recovery system with loop transmission modulus reduction compensation in the quiescent condition are compared to an alternative approach of strict modulus reduction via nonlinear compensation for stability retention. Efficacy of the loop recovery approach is illustrated using experimental data from a voice-coil actuated disturbance rejection system.

Keywords: Feedback control, imperfect actuators, nonlinear dynamic compensation

DOI https://doi.org/10.1007/s11768-019-8031-y

1 Introduction

Large feedback control systems require accurate plant models for purposes of design. While large feedback has the effect of reducing sensitivity to small parameter variations in the actuator, nonlinearities such as those found in inexpensive actuators affect changes in loop gain that threaten stability. This is an unfortunate limitation, as cheaper actuators are typically more rugged than their expensive counterparts and are more suited to military applications where large disturbance rejection is often required. A method for large feedback control applied to quasi-linear plants is presented. Such plants are characterized by disjoint input intervals where superposi-

†Corresponding author.

E-mail: obrieny@uwyo.edu.

This work was supported by the U.S. Department of Energy (No. DE-SC0012671).

tion fails. Inside these intervals nonlinear features govern the response. These nonlinearities can be classified as *limit* nonlinearities such as actuator saturation, and *imperfection* nonlinearities, commonly friction/stiction nonlinearities in moving parts of a mechanical system. When there are variations in loop gain and phase which these nonlinearities produce, high performance linear controllers designed for large feedback will oscillate. To satisfy the high performance requirement, conventional methods of improving robustness such as bandwidth reduction and shallow loop transmission roll-off are not applicable. Instead direct compensation of the effects of these nonlinear features in the high performance controller design is prudent.

The area of constrained control is well researched, yet most attention is given to the issue of wind-up in saturated loops with integral action. An ample overview of the anti-windup control problem in both its previous and subsequent alternatives is given in [1,2]. In these papers the connection between anti-windup control and stabilizing control to satisfy the absolute stability condition is established. Contemporary anti-windup theory can be described as the application of modern and robust control theory to the constrained problem [3, 4] and [5, 6]. A control architecture that trades high performance for increased robustness in saturation is presented in [7]. Stability of feedback controllers applied to systems with hard or limiting nonlinearities confined to sectors can be assessed using absolute stability theory [8, 9]. A Popov-like criterion is used in a control design for a system with non-collocated actuators and friction in [10]. Nyquist-stable control applied to the spaceborne interferometer pathlength regulation problem is described in [11, 12]. Nonlinear dynamic compensation with multiple feedback paths is applied to a marine autopilot with steep loop transmission roll off and multiple actuator saturations in [13, 14]. In an aggressive feedback system such compensator is used to smoothly vary loop transmission in order to retain stability. Its implementation is similar to variable gain control approach to adjust loop transmission as a function of disturbance-driven error. A variable gain scheme is applied to optical disk drives in [15], and facilitates a smooth transfer of loop gain between channels of a single-input/two-output wind turbine rate regulator in [16, 17] and also in [18].

There is a long history in the study of controlled systems with friction; comprehensive analysis is found in [19,20] and in [21,22]. In specific cases the effect of friction is well known, however a general theory explaining all friction phenomenon has yet to be developed [23]. One of the earliest investigations of servomechanisms with friction uses describing function analysis [24]. The results demonstrate that friction imposes limitations on the amount of feedback available with linear control. A closed-loop system response shows limit cycle oscillations when a more aggressive controller is applied. An algebraic analysis in [25] finds that PID control of systems with certain friction nonlinearities, minimal Coulomb and nonzero static frictions also exhibits limit cycling. Control application to compensate this nonlinear behavior is desired in order to ameliorate negative effect of friction on system response. Several nonlinear modifications to PID control and adaptive control strategies to compensate for friction are described in [20]. PID, PID with dithering, and three adaptive controllers using different friction models are implemented and compared to conclude that the Dahl model is the most suitable. A learning control scheme to track trajectories in mechanical systems with friction is discussed in [26]. A method of adaptive nonlinear friction compensation is presented in [27]. The design is a PD controller with reversed position-error integral control proving to be effective at compensating for Coulomb-like friction in a 6-degrees of freedom (6-DOF) manipulator. The friction model of [19] is utilized in a PID control scheme for a second order mechanical system with perfect knowledge in [28]. To compensate for Coulombic friction in single DOF mechanical system with friction an adaptive control method is used in [29]. Adaptive friction compensation is applied using extended Kalman-Bucy filter friction estimation to a simple rotary plant in [30]. Sliding-mode control has been used on a second-order mechanical systems with friction [31, 32]. Simulation results show accurate tracking of sinusoidal signal of a flight simulation table in a noiseless environment. To reduce stack overflow in hysteresis force application modifications to the Leuven friction and Maxwell slip models are made in [33]. High performance motion tracking feedforward control of the art laser processing system for electronics manufacturing is experimentally researched in [34]. A controller is designed using an approximate nonminimum-phase LTI model of the closed-loop plant, inverse dynamics control, an adaptive FIR filter, and an iterative learning control algorithm. A wide variety of research done in the area implies a canonical set of friction models for control applications does not yet exist. Furthermore, these approaches for modeling and control of plants with friction are developed for low

performance improvements in small disturbance environments, and are ill-suited for aggressive controllers subjected to large disturbance power.

An approach that employs nonlinear dynamic compensation (NDC) with multiple feedback paths to allow the stable application of large feedback despite multiple loop nonlinearities is presented in [35, 36]. While the work focused on smooth transitions of transmission to loop shapes that satisfy the conditions of absolute stability, the notion of using nonlinear compensation to *increase* loop modulus to reestablish the aggressive shape designed for nominal operation was introduced. This approach does not compromise feedback applied over the functional bandwidth in the nominal disturbance environment, however initial experiments showed that this method of nonlinear compensation produced excessive positive feedback in the neighborhood of crossover. Such a limiting feature of the gain-increasing nonlinear compensation scheme is considered by authors a potentially unacceptable.

The *parallel loop recovery* (PLR) system for nonlinear loop transmission reintroduction with acceptable positive feedback is presented in this paper. It is shown that the decomposition of the low amplitude input subdomain into intervals for individual nonlinear compensation designs provides the necessary design degrees-of-freedom for the accurate reshaping of the loop transmission. The PLR system is augmented with *quiescent compensation* to further improve response characteristics when operating in very low disturbance power conditions where loop modulus augmentation is very difficult to realize. The efficacy of the approach is shown using data acquired in an in-depth experimental case study on a parallel robot articulation system.

Requisite terminology and background theory are presented in Section 2. A definition of plants that are *linear on an interior input domain* is provided in Section 3. Four nonlinear dynamic compensation schemes for operation on such systems, with an emphasis on PLR, are described in Section 4. A stability analysis is discussed in Section 5. Section 6 provides details of the design and experimental verification of the PLR system. The Nyquist-stable control system described delivers 38 dB of feedback over a 10 Hz functional bandwidth with only a 40 Hz control bandwidth. Further, it retains stability when the actuator saturates and when the system is influenced by uncertain nonlinearities in the small-signal condition, features a linear Nyquist-stable system does not possess.

2 Preliminaries

2.1 Terminology

For the feedback loop in Fig. 1, rational function $T(s) = C(s)P(s)A(s) = \dfrac{u_2(s)}{u_1(s)}$ of the Laplace variable s is the loop transmission (alternatively return ratio) of a feedback loop. In this expression, $C(s)$ is the controller, $P(s)$ is the transfer function of the plant, and $A(s)$ models the actuator dynamics. For a low pass loop transmission, ω_b where $|T(j\omega_b)| = 1$ is the *control bandwidth* (alternatively *0 dB crossover frequency*). Define ω_f where loop transmission modulus is constant, i.e., $|T(j\omega)| \simeq T_0$, $\forall \omega \leqslant \omega_f$, as the *functional bandwidth*. $|F(s)| = |1+T(s)|$ is the feedback. $|F(s)| > 1$, $|F(s)| < 1$ and $|T(s)| \ll 1$ define *negative*, *positive* and *negligible* feedback, respectively. $|F(s)| \gg 1$ defines *large* feedback, a critical inequality that the linear controllers described in this paper satisfy over the functional bandwidth. These definitions indicate the effect of feedback on the logarithmic response of the closed-loop system to disturbances. *Nonminimum phase* is the phase lag not found using the Bode phase/gain relationship [37]. A feedback system is *Nyquist-stable* if $T(s)$ is stable, satisfies the Nyquist Criterion, and rolls off at a slope steeper than $-12\,dB/oct$ over an interval of frequencies less than ω_b. $\mathbb{R}_+$ and $\mathbb{R}_{+0}$ are the positive and non-negative real numbers. $\mathbb{R}^{m\times n}(s)$ is the $m \times n$ matrix of rational functions of the Laplace variable.

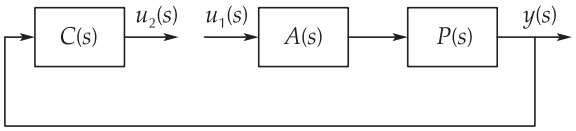

Fig. 1 Feedback system opened in the forward path.

2.2 Background theory

Consider an unforced nonlinear system

$$\dot{x} = Ax + Bu, \tag{1}$$

$$y = Cx, \tag{2}$$

$$u = -\psi(y), \tag{3}$$

where $x \in \mathbb{R}^n, u, y \in \mathbb{R}^p, (A, B)$ is controllable, (A, C) is observable, and $\psi : [0, \infty) \times \mathbb{R}^p \to \mathbb{R}^p$ is memoryless, possibly time-varying, nonlinearity which is piecewise continuous in t and locally Lipschitz in y. The resulting

transfer function matrix of the linear system is given by

$$T_{\text{eq}}(s) = C(sI - A)^{-1}B, \tag{4}$$

which is a square strictly proper transfer function. The nonlinearity $\psi(y)$ is required to satisfy a *sector condition*, i.e.,

$$[\psi(y) - K_{\min}y]^{\text{T}}[\psi(y) - K_{\max}y] \leqslant 0, \quad \forall y \in \Gamma \subset \mathbb{R}^p \tag{5}$$

for some real matrices $K_{\min}$ and $K_{\max}$, where $K = K_{\max} - K_{\min}$ is a positive definite symmetric matrix and the interior of Γ is connected and contains the origin. If $\Gamma = \mathbb{R}^p$, then $\psi(y)$ satisfies the sector condition globally, and it is said that $\psi(y)$ belongs to a sector $[K_{\min}, K_{\max}]$ [9].

The system in equations (1)–(3), where $\psi(y)$ satisfies a sector condition in equation (5), is *absolutely stable* if the origin is globally uniformly asymptotically stable for any nonlinearity in the given sector. It is absolutely stable with a finite domain if the origin is uniformly *asymptotically stable* [9]. The *asymptotic stability* condition of the origin is established in Lyapunov's stability theorem [9].

3 Actuator domain intervals

Consider the SISO system to be controlled consisting of a rational function model of linear system $P(s)$ in cascade with the actuator modeled by operator $A(u)$. Define the disjoint sets

$$\begin{aligned}
\mathscr{U}_1 &= \{u : |u| \leqslant \bar{u}_1\},\\
\mathscr{U}_2 &= \{u : \bar{u}_1 < |u| \leqslant \bar{u}_2\},\\
\mathscr{U}_3 &= \{u : |u| > \bar{u}_2\}.
\end{aligned}$$

For actuators considered in this work, $A(u)$ satisfies superposition in $u \in \mathscr{U}_2$ and does not hold for inputs in $\mathscr{U}_1 \cup \mathscr{U}_3$. Inputs in $\mathscr{U}_2$ are considered in the nominal operating domain, those in $\mathscr{U}_3$ overdrive the actuator, and those in $\mathscr{U}_1$ are sufficiently small so that the response is substantially influenced by actuator imperfections (e.g., stiction).

4 Nonlinear dynamic compensation schemes

Nyquist-stable control is sensitive to changes in loop gain, as adequate margins of stability are usually established over narrow frequency intervals. Shifts in loop gain caused by actuator nonlinearities will produce oscillations, and as such its application to systems with nonlinear actuators is particularly dangerous. The actuator typically has reduced gain in response to inputs in intervals $\mathscr{U}_1$ and $\mathscr{U}_3$ compared to those in $\mathscr{U}_2$ for which the linear compensator for the Nyquist-stable controller is designed, and stability is threatened as discussed previously. The nonlinear feedback connections between $C(s)$ and $A(u)$ shown in Fig. 2 make up the NDC, designed to reshape the loop transmission in $\mathscr{U}_1 \cup \mathscr{U}_3$ to retain stability and performance.

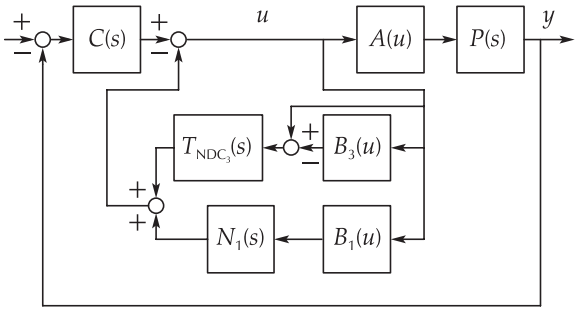

Fig. 2 Block diagram of the NDC.

The designer often knows $A(u)$ exactly for $u \in \mathscr{U}_3$ as this is usually a saturation, but not for $u \in \mathscr{U}_1$. Nonlinear dynamic compensation for the known actuator saturation limits (consisting of systems T_{NDC_3} and B_3) must be implemented to avoid oscillations when overdriven. Details of such a design is found in [38]. A design for the N_1 NDC path is proposed with the assumption that the uncertain $\mathscr{U}_1$ nonlinearities reduce actuator responsiveness, and the output is on or below the unit gain line. As such, it can be assumed that $A(u)$ is confined to the sector [0 1] for $u \in \mathscr{U}_1$. It is noted that if the designer has *a priori* knowledge that loop nonlinearities are not confined to this sector, a larger sector must be selected that subsumes all expected functions.

As the interval $\mathscr{U}_1$ is not exactly known, engineering judgment is used to select parameter $\bar{u}_{1\text{e}}$ as an estimate of this width to define function $B_1(u)$,

$$B_1(u) = \begin{cases} u, & |u| \leqslant \bar{u}_{1\text{e}},\\ \bar{u}_{1\text{e}}\operatorname{sgn} u, & \text{otherwise.} \end{cases} \tag{6}$$

The parameter should be selected so $\bar{u}_{1\text{e}} > \bar{u}_1$, but not so large that the NDC is heavily active in $u \in \mathscr{U}_2$.

It is assumed that the actuator limit, $\bar{u}_{\text{act}}$, is a known parameter used to define $B_3(u)$.

$$B_3(u) = \begin{cases} u, & |u| \leqslant \bar{u}_{\text{act}}, \\ (\bar{u}_{\text{act}})\operatorname{sgn} u, & \text{otherwise.} \end{cases} \tag{7}$$

It is reasonable to require $\bar{u}_{1\text{e}} < \bar{u}_{\text{act}}$ (the set of small-signal inputs and the set of inputs that overdrive the actuator are disjoint), and so the NDC paths associated with the B_1 and B_3 systems are not simultaneously active.

4.1 Gain-decreasing nonlinear dynamic compensation (GDNDC)

The complete NDC system consists of two nonlinear designs that are active in small and large signal conditions, the $\mathscr{U}_1$ and $\mathscr{U}_3$ NDCs, respectively. The NDC of Fig. 2 may be designed to reduce the loop transmission so that $T_{\text{eq}}(s)$, the equivalent linear system in feedback connection to the nonlinear system $A(u)$, satisfies the conditions of absolute stability [9] with the condition $A(u)$ confined to a given sector (in this work, the sector is [0 1]); this is referred to as a *gain-decreasing* nonlinear dynamic compensator [36].

4.1.1 $\mathscr{U}_1$ NDC

Consider the loop transmission function,

$$T_{\text{AS}}(s) = C_{\text{AS}}(s)P(s), \tag{8}$$

where $P(s)$ is a transfer function model of the plant dynamics in the linear condition, and $C_{\text{AS}}(s)$ is the compensator such that $T_{\text{AS}}(s) = T_{\text{eq}}(s)$ satisfies the conditions of absolute stability for the given sector. For $|u| \leqslant \bar{u}_{1\text{e}}$, the system of Fig. 2 is equivalently a feedback connection of the sector nonlinearity with a linear system having the following transfer function.

$$\frac{P(s)C(s)}{1 + N_1(s)} = T_{\text{eq}}(s). \tag{9}$$

$C(s)$ is the compensator designed for linear operation (i.e., $T(s) = C(s)P(s)$, a high performance loop transmission that lacks absolute stability over sufficiently wide sectors). If $T_{\text{eq}}(s) = T_{\text{AS}}(s)$, the resulting feedback system is absolutely stable on the finite domain $|u| \leqslant \bar{u}_{1\text{e}}$. This is the GDNDC.

4.1.2 $\mathscr{U}_3$ NDC

It is assumed that B_3 is an accurate model of the actuator saturation. As such, the outputs of systems A and B_3 are equal, and the transfer function of the equivalent linear system in feedback connection to the sector nonlinearity is as follows:

$$\frac{P(s)C(s) - T_{\text{NDC}_3}(s)}{1 + T_{\text{NDC}_3}(s)} = T_{\text{eq}}(s). \tag{10}$$

If $A(u) = B_3(u)$ and $T_{\text{NDC}_3}(s)$ is selected such that $T_{\text{eq}}(s) = T_{\text{AS}}(s)$, then the $\mathscr{U}_3$ NDC would alone provide stability. However, the saturation function does not model the effects of the $\mathscr{U}_1$ nonlinearities and the $\mathscr{U}_3$ NDC does not compensate for them, thus necessitating the inclusion of the $\mathscr{U}_1$ NDC described previously. Experimental data indicating the necessity of multiple-path NDC for imperfect actuators is provided in the sequel.

4.2 Gain-increasing nonlinear dynamic compensation (GINDC)

In contrast to the gain-reduction approach, the focus of this work is the implementation of nonlinear dynamic compensation to *re-introduce* loop gain lost to mechanism imperfections in the system. The GINDC seeks to reestablish the original Nyquist-stable loop shape when $u \in \mathscr{U}_1$ (referring to Fig. 2, this is the loop transmission $C(s)P(s)$ in $\mathscr{U}_2$). In this case, the $B_1(u)$ nonlinear function is identical to the gain-decreasing NDC, however the rational function $N_1(s)$ is found with a different goal in mind. In the gain-increasing design, $N_1(s)$ is found so that

$$\frac{P_1(s)C(s)}{1 + N_1(s)} = C(s)P(s), \tag{11}$$

where $P_1(s)$ is the transfer function model of the actuator/plant response under the influence of the $\mathscr{U}_1$ nonlinearities. This approach reestablishes the Nyquist-stable loop shape ($C(s)P(s)$) for the particular response modeled by $P_1(s)$, and the closed-loop system will have greater disturbance rejection than the gain-decreasing NDC. While $C(s)P(s)$ satisfies the Nyquist Stability Criterion, the system with gain-increasing nonlinear compensation that reestablishes this loop shape clearly does not satisfy the sufficient condition of absolute stability for the [0 1] sector in the finite domain $|u| \leqslant \bar{u}_{1\text{e}}$. This illustrates the contrast in the GDNDC and GINDC approaches to nonlinear dynamic compensation: the former satisfies conservative absolute stability conditions, the latter directly compensates for the effects of loop nonlinearities to retain high performance.

4.3 Parallel loop recovery (PLR)

For GINDC, $N_1(s)$ is designed using a frequency response measurement of the plant for a selected $\mathscr{U}_1$ input ($P_1(s)$ models this) so that the original Nyquist-stable loop transmission is reestablished. However, plant frequency responses in $\mathscr{U}_1$ may be quite sensitive to input amplitudes in this interval due to contact type nonlinearities, e.g., stiction. Hence, the GINDC design may perform well for control signals similar to the test signal, and poorly for other signals in $\mathscr{U}_1$. Considering the reestablished loop shape is Nyquist-stable, the sensitivity to errors in the recovered loop transmission include the plant model modulus being either too high or too low (in both cases, excessive positive feedback may result).

More accurate reshaping of the loop in $\mathscr{U}_1$ is established with the PLR system shown in Fig. 3 (without the quiescent compensator to be described in the sequel). As opposed to one model of the plant response in $\mathscr{U}_1$, multiple models of the plant are identified at different input amplitudes, and associated NDC gain-increasing systems are designed. The linear systems $N_{1i}(s)$ for PLR satisfy the following equality condition:

$$\frac{P_j(s)C(s)}{1+\sum_{i=1}^{j} N_{1i}(s)} = C(s)P(s) \tag{12}$$

for $m\mathscr{U}_1$ plant responses of diminishing modulus at low frequency (i.e., for ω_1 less than the control bandwidth, $|P_i(\mathrm{j}\omega_1)| > |P_{i+1}(\mathrm{j}\omega_1)|$, $i = 1, 2, \ldots, m-1$).

The associated nonlinear functions $B_{1i}(u)$ are described by the following equation:

$$B_{1i}(u) = \begin{cases} u, & |u| \leqslant u_{1i}, \\ u_{1i}\operatorname{sgn} u, & \text{otherwise.} \end{cases} \tag{13}$$

Threshold values are selected using observations of system responses and engineering judgment, and satisfy $u_{11} > u_{12} > \ldots > u_{1m} > 0$.

4.4 Parallel loop recovery with quiescent compensation (PLRQC)

PLR restores large loop transmission in $\mathscr{U}_1$ through blended compensation designed using black box models of the system frequency response to selected low amplitude inputs. Imperfect actuators, for example, those exhibiting stick/slip characteristics, respond in very low $\mathscr{U}_1$ dramatically differently than they do to larger amplitude inputs. For such systems, the model quality is poor, and the aggressive design approach to reestablish large feedback in this condition is contraindicated, as the resulting loop shape may not be what the designer intended. An additional consideration is that large feedback in this condition is not necessary as the disturbance power is likely very low.

For such systems, PLR is modified to include *quiescent compensation*, whereby a subset of the $\mathscr{U}_1$ NDC linear systems associated with compensation in the lower signal amplitudes are designed to *reduce* loop transmission as opposed to increase it. A block diagram of the PLRQC is shown in Fig. 3. NDC systems $N_{11}(s)$ through $N_{1(m-1)}(s)$ are loop recovery systems described previously to reestablish the Nyquist-stable loop shape for high $\mathscr{U}_1$ inputs. System $N_{1m}(s)$ reduces loop transmission for low $\mathscr{U}_1$ inputs. PLRQC trades feedback for increased robustness in the quiescent (or near-quiescent) operating condition, and as such, slightly reduced disturbance rejection is expected over the functional bandwidth in the nominal operating condition.

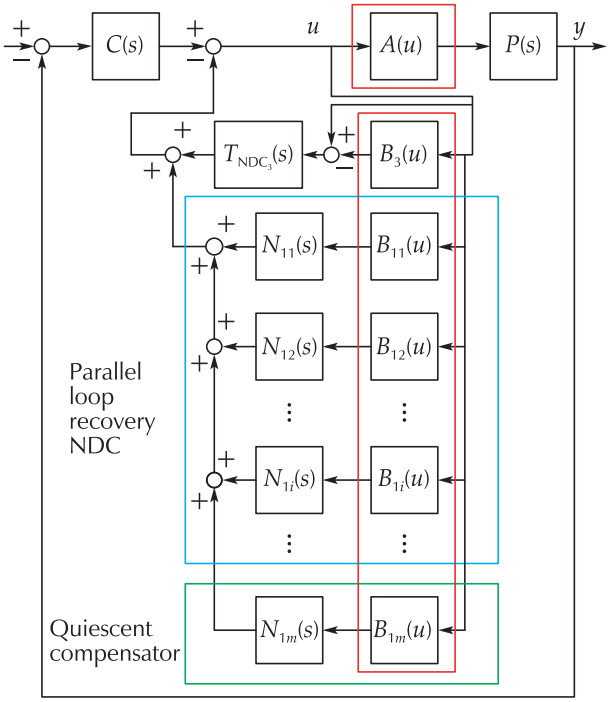

Fig. 3 Parallel loop recovery nonlinear dynamic compensator with quiescent compensation.

5 Stability analysis

Considering the system possesses uncertain nonlinear subsystems, the *absolute stability* of the feedback

system is assessed over sectors to which these nonlinearities are assumed to be limited [9]. For the case of $\mathscr{U}_3$ NDC only (Section 4.1.2) to provide stability in the presence of actuator saturation (the only nonlinearity in the system), $B_3(u) = A(u) = \text{sat}(u)$, and absolute stability of the single-input and single-output (SISO) system can be determined using the Nyquist or Popov plots of $T_{\text{eq}}(s)$ in equation (10). The introduction of an uncertain nonlinearity (one for which an equation is not available, however memorylessness and confinement to a particular sector is assumed) in the forward path with attendant nonlinear NDC paths (i.e., $\mathscr{U}_1$ gain-decreasing and gain-increasing systems) complicates absolute stability assessment, and despite the system being SISO, an alternative analysis is indicated.

For the $\mathscr{U}_1$ NDC systems, the loop is treated as a multiple-input and multiple-output (MIMO) system shown in Fig. 3. The systems of Figs. 2 and 3 are re-expressed as $(m + 2) \times (m + 2)$ (m the number of $\mathscr{U}_1$ NDC paths) MIMO feedback systems. Lower and upper sector bounds for each decoupled channel reside on the diagonals of diagonal matrices $K_{\min}$ and $K_{\max}$, respectively.

The $\mathbb{R}^{(m+2)\times(m+2)}(s)$ transfer matrix, $T_{\text{eq}}(s)$, for the equivalent linear system in feedback connection to the nonlinear system has identical rows consisting of

$$\frac{1}{1 + T_{\text{NDC}_3}(s)} \begin{bmatrix} P(s)C(s) \\ N_{11}(s) \\ N_{12}(s) \\ \vdots \\ N_{1m}(s) \\ -T_{\text{NDC}_3}(s) \end{bmatrix}^{\text{T}}. \tag{14}$$

The nonlinear feedback system is *absolutely stable* if the origin is asymptotically stable for any nonlinearity in the sector $[K_{\min}\ K_{\max}]$ [9]. An application of Lyapunov's basic theorem and the Kalman-Yakubovich-Popov Lemma, the *Multivariable Circle Criterion* establishes a sufficient condition for absolute stability [9].

1) Sector condition (5) is satisfied;

2) $M(s) = T_{\text{eq}}(s)[I + K_{\min}T_{\text{eq}}(s)]^{-1}$ is stable; and

3) $Z_T(s) = [I + K_{\max}T_{\text{eq}}(s)][I + K_{\min}T_{\text{eq}}(s)]^{-1}$ is strictly positive real.

The stability of system $M(s)$ (item 2) is determined graphically using the *Generalized Nyquist Theorem* [39] (the characteristic loci of loop transmission matrix $K_{\min}\times T_{\text{eq}}(s)$ must encircle the critical point P_0 times anticlockwise (P_0 the number of unstable Smith-McMillan poles of $T_{\text{eq}}(s)$)). Proper, square rational transfer matrix $Z_T(s)$ is strictly positive real (item 3) if

1) All poles of elements of $Z_T(s)$ have negative real parts;

2) $Z_T(\text{j}\omega) + Z_T^{\text{T}}(-\text{j}\omega) > 0, \forall\omega \in \mathbb{R}$; and

3) $Z_T(\infty) + Z_T^{\text{T}}(\infty) > 0$.

6 Experimental case study

The control approach is tested on a parallel mechanism with two degrees of freedom (two-DOF parallel mechanism) shown in Fig. 4, developed as part of an ongoing investigation of the implementation of parallel robots in vibration suppression applications [40, 41], followed by [38, 42] and [43, 44]. The control goal is to provide as much disturbance rejection as is feasible subject to practical limitations. While the mechanism has two-DOF, the experiment will focus on only one of these, namely the regulation of the voice coil (prismatic actuator) at its home configuration. The unique architecture decouples the task DOFs, and as such, similar control can be applied to the second actuator.

As large disturbance rejection is required, a Nyquist-stable controller with nonlinear dynamic compensation is designed. System identification indicates that while the mechanism responses are principally linear, imperfection nonlinearities cause an undesired reshaping of the plant frequency response at low input amplitudes. Two NDC design approaches are investigated in details:

1) NDC reshapes the loop for less aggressive feedback in $\mathscr{U}_1 \cup \mathscr{U}_3$ (gain-decreasing NDC).

2) PLRQC.

The PLRQC compensator has higher performance than GDNDC as it is a partially gain-increasing scheme. The reduction in localized positive feedback of the PLRQC system when compared to a strictly gain increasing system (GINDC or PLR) is evident in data presented in the sequel.

6.1 Section terminology

Exogenous disturbances are applied to the feedback system are zero mean Gaussian signals input to the actuator driver in levels defined by rms: Levels 0 and 1 are very low (variance of Level 0 signal less than that of Level 1), generating control inputs in $\mathscr{U}_1$; Level 2 is low, generating control inputs in both $\mathscr{U}_1$ and $\mathscr{U}_2$, Level 3 is nominal, generating inputs principally in $\mathscr{U}_2$; and Level 4

is high, frequently generating amplitudes exceeding the control signal limit set in software at ±0.2 V.

6.2 Plant architecture

The plant is a PUS – RR parallel robot shown in Fig. 4. One kinematic path consists of an active prismatic actuator (a linear voice coil manufactured by BEI Kimco Magnetics Division, model number LA28-43-000A), universal joint, and sphere joint (PUS). The coil is mechanically in series with helical springs that provide a restoring force to keep the end-effector centered when unpowered. The other DOF is made available by a series connection of an active revolute actuator (brushless DC servo motor manufactured by Teknic) and a pin joint (RR). This DOF is not used for the control experiments described in this paper. A Helium-Neon (HeNe) laser is used in conjunction with an ON-TRAK Photonics OP-324 position sensitive detector (PSD) to measure the end-effector position. The absolute and differential kinematics of the system are described in [41].

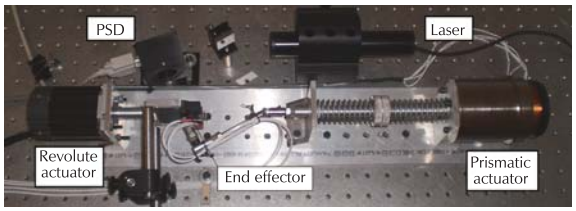

Fig. 4 PUS – RR parallel robot.

6.3 System identification

The prismatic actuator is driven with white noise of sufficient variance for system identification in $\mathscr{U}_2$. The stimulus and end-effector position signals are digitized and recorded using an Agilent VXI system. The data is processed using the SignalCalc 6.2 software suite from DataPhysics. A pole-zero-gain (PZK) model of the plant $P(s)$ is developed by the placement of poles and zeros so that the $P(s)$ frequency response mimics that of the experimental data. $P(s)$ is the 15th order; the gain K, zeros s_z, and poles s_p of $P(s)$ are given in Table 1. The frequency response is plotted along with the experimentally acquired data in Fig. 5.

It is desired to gain-stabilize all high-frequency modes in the plant. This constraint along with the third-order roll-off of the plant response starting in the 50–100 Hz interval forces a control bandwidth of approximately 40 Hz. A 10 Hz functional bandwidth is desired, thus allowing only two octaves between the loop transmission break and crossover, necessitating a Nyquist-stable loop shape to achieve high performance.

Table 1 PZK model of the plant $P(s)$.

K	s_z	s_p
4.4×10^{20}	−5027	−25.13
	−2.482 ± 496.4i	−24.82 ± 495.8i
	−904.8 ± 2877i	−301.6 ± 402.1i
	−904.8 ± 2877i	−1319 ± 2285i
	−108.1 ± 5402i	−184.7 ± 2632i
		−257.6 ± 5146i
		−457.4 ± 6518i
		−326.7 ± 8162i

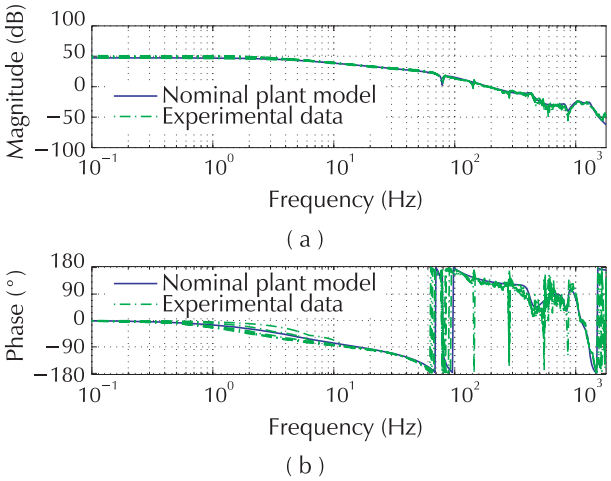

Fig. 5 PUS – RR plant frequency response.

6.4 Nyquist-stable compensator design

A high performance *Nyquist-stable* controller $C(s)$ is designed with the goal of providing large disturbance rejection at frequencies below the 10 Hz functional bandwidth. $C(s)$ is designed using the *loop shaping* method whereby compensator poles and zeros are chosen to warp $T(s) = C(s)P(s)$ to the desired shape:

. A zero at 4 Hz flattens the response below the 10 Hz functional bandwidth.

. Conjugate pole pairs at 7 Hz and 10 Hz provide the break at the functional bandwidth.

. The pole pair at 10 Hz and a zero pair at 15 Hz provide the sharp transitions seen in the slope of the loop transmission in this frequency interval.

. A pair of zeros at 60 Hz and a pair of poles at 200 Hz flatten the response.

. A two octave wide lead filter centered at 100 Hz further flattens the response and adds phase lead.

. The loop shape is such that the positive feedback never exceeds 6 dB.

. The gain, zeros, and poles of $C(s)$ are presented in Table 2.

The resulting 7th order compensator provides approximately 38 dB of disturbance rejection below 10 Hz (63 rad/s), as seen in the Nichols plot of $C(s)P(s)$ shown in Fig. 6. The control bandwidth is approximately 40 Hz (251 rad/s).

Table 2 PZK model of the compensator $C(s)$.

K	s_z	s_p
2119	−25.13	−1257
	−314.2	−33.93 ± 25.45i
	−14.14 ± 93.18i	−12.57 ± 61.56i
	−188.5 ± 326.5i	−1257 ± 2177i

The controller oscillates in saturation ($\mathscr{U}_3$) and in response to low disturbance power ($\mathscr{U}_1$), necessitating a multiple-loop NDC to provide absolute stability.

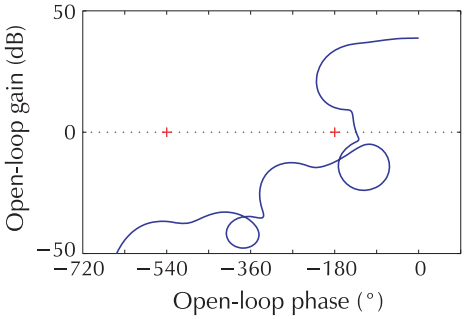

Fig. 6 Nyquist-stable controller loop transmission.

6.5 System identification 2: plant response to low input power

The plant frequency response moduli for six input rms values from 0.01–0.60V_{rms} are shown in Fig. 7. Within a few dB of each other, the inputs associated with the green (0.4V_{rms}) and dark blue functions (0.6V_{rms}) are considered principally in $\mathscr{U}_2$, or what is expected in nominal mechanism operation. Larger input amplitudes that do not saturate the actuator result in frequency responses that roughly overlap the blue function, suggesting the system is very nearly linear and is treated as such for these inputs.

It is noted that responses to input amplitudes from 0.05–0.20V_{rms} have reduced moduli at frequencies below 200 Hz (several octaves higher than the control bandwidth). The slope is roughly first order for all responses, and the only significant difference below 100 Hz is the zero-pole combination at 80 Hz associated with the helical spring. As such, the imperfections of the plant primarily affect a *gain* shift in the plant response. The response to the 0.01V_{rms} input, however, significantly differs in that it is zero slope. This response suggests the dominant effects of joint imperfections in the nearly quiet condition.

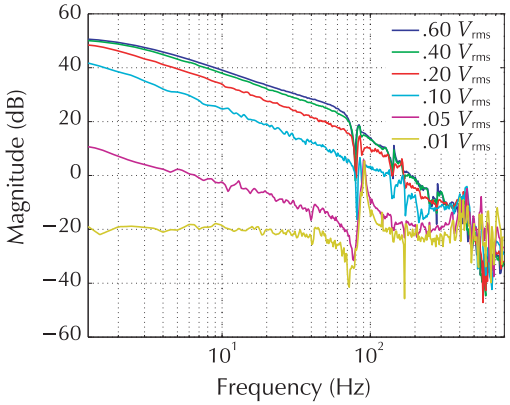

Fig. 7 Plant response to zero-mean white noise stimulus of different variances.

The plant satisfies (in an approximate sense) superposition for what can be termed "mid-range" input amplitudes, responds nonlinearly to small signals, and saturates when driven by large signals. The first step in the control development is the design of a Nyquist-stable controller for the mid-range response with nonlinear dynamic compensation for actuator saturation. After verifying the required attenuation of the effect of exogenous forces on the robot pose with inputs principally in $\mathscr{U}_2$ and stability in saturation ($u \in \mathscr{U}_3$), the effects of operation in $\mathscr{U}_1$ are evaluated and additional nonlinear compensation is designed.

6.6 $\mathscr{U}_1$ gain decreasing nonlinear dynamic compensator design

A single path, gain decreasing NDC is designed. Referring to Fig. 3, the NDC consists of linear systems $T_{\text{NDC}_3}(s)$ and $N_{11}(s)$ ($N_1(s)$ in Fig. 2 and nonlinear systems $B_3(u)$ and $B_{11}(u)$. The gain, zeros, and poles of $T_{\text{NDC}_3}(s)$ are given in Table 3.

$B_3(u)$ is the saturation nonlinearity with a limit of 0.2 (this is the limit of the voice coil) [38]. The gain, zeros, and poles of $N_{11}(s)$ for the gain-decreasing $\mathscr{U}_1$ NDC are presented in Table 4. $B_{11}(u)$ is the saturation function with limit 0.0055. The gain, zeros, and poles of compensator $C_{\text{AS}}(s)$ are summarized in Table 5.

Table 3 PZK model of the $T_{\mathrm{NDC}_3}(s)$.

K	s_z	s_p
		−222.1
	−1777	−33.93 ± 25.45i
1.66×10^{12}	−46.37 ± 61.83i	−15.71 ± 60.84i
	−37.7 ± 119.9i	−942.5 ± 1257i
		−377 ± 2485i

Table 4 PZK model of the $N_{11}(s)$.

K	s_z	s_p
		−222.1
	−1777	−33.93 ± 25.45i
1.66×10^{12}	−46.37 ± 61.83i	−15.71 ± 60.84i
	−37.7 ± 119.9i	−942.5 ± 1257i
		−377 ± 2485i

Table 5 PZK model of the $C_{\mathrm{AS}}(s)$.

K	s_z	s_p
2119	-0.0251×10^3	-1.2570×10^3
	-0.2221×10^3	-0.4038×10^3
	-0.3142×10^3	$(-0.0472 \pm 0.0547\mathrm{i}) \times 10^3$
	$(-0.0157 \pm 0.0608\mathrm{i}) \times 10^3$	$(-0.0126 \pm 0.0616\mathrm{i}) \times 10^3$
	$(-0.0141 \pm 0.0932\mathrm{i}) \times 10^3$	$(-0.0094 \pm 0.0967\mathrm{i}) \times 10^3$
	$(-0.1885 \pm 0.3265\mathrm{i}) \times 10^3$	$(-0.8440 \pm 1.3628\mathrm{i}) \times 10^3$
	$(-0.9425 \pm 1.2570\mathrm{i}) \times 10^3$	$(-1.2570 \pm 2.1770\mathrm{i}) \times 10^3$
	$(-0.3770 \pm 2.4850\mathrm{i}) \times 10^3$	$(-0.3777 \pm 2.4026\mathrm{i}) \times 10^3$

Sectors are selected for absolute stability analysis. As there are three nonlinearities in this system (actuator nonlinearity in the forward path $A(u)$, and two NDC nonlinear functions $B_{11}(u)$ and $B_3(u)$), the matrices defining the upper and lower limit ($K_{\max}$ and $K_{\min}$, respectively) for a given sector are $\mathbb{R}^{3\times3}$. These matrices are chosen to be diagonal with individual channel limits ordered thusly: the $(1,1)$ entries define the sector to trap $A(u)$, the $(2,2)$ entries correspond to $B_{11}(u)$, and the $(3,3)$ entries correspond to $B_3(u)$. It is noted that the NDC nonlinearities are known functions, while $A(u)$ is not. The analysis seeks to determine finite domains over which the 3×3 system satisfies the Circle Criterion.

Absolute stability analysis is presented for this system. Satisfaction of the conditions of the Multivariable Circle Criterion listed in Section 5 for this system are verified for two sectors $[K_{\min_i} \ K_{\max_i}]$, $i = 1, 2$.

6.6.1 Sector 1

Sector 1 is $K_{\min_1} = \mathrm{diag}\{0,\ 0.9,\ 0.9999\}$, $K_{\max_1} = \mathrm{diag}\{0.33, 1, 1\}$. This sector is selected to determine stability for small signal nonlinear responses of $A(u)$ (for this case, the system is stable for any nonlinearity in the sector [0 0.33]). Fig. 8 shows the characteristic loci for $K_{\min_1} T_{\mathrm{eq}}(s)$; there are no encirclements of the critical point (−1+j0) and as the open loop system is stable, $M(s)$ is stable by the Generalized Nyquist Theorem (condition (2) in Section 5. Fig. 9 shows the minimum eigenvalues of $Z(\mathrm{j}\omega) + Z^{\mathrm{T}}(-\mathrm{j}\omega)$ as a function of frequency, showing that conditions (2) and (3) for strict positive reality in Section 5 are satisfied (all poles of $Z(s)$ have negative real parts, condition (1)), thus condition (3) of the Circle Criterion is satisfied and the system is absolutely stable over this sector. Recall the $B_{11}(u)$ is the saturation with limit 0.0055, so the lower sector limit of 0.9 intersects this at $u = \pm 0.0061$, and thus this is the domain for which the system is absolutely stable for this sector (approximately 3 percent of the actuator range).

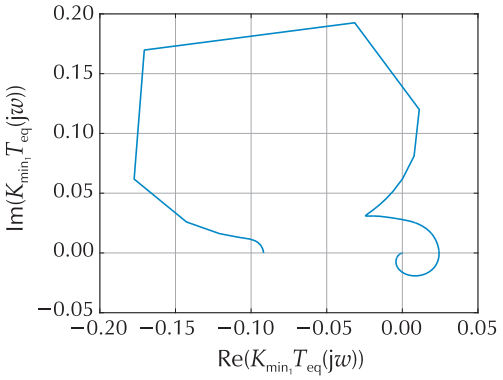

Fig. 8 Characteristic loci $K_{\min_1} T_{\mathrm{eq}}(s)$ for the $\mathscr{U}_3$ and gain-decreasing $\mathscr{U}_1$ NDC. Two of the three loci are very small magnitude.

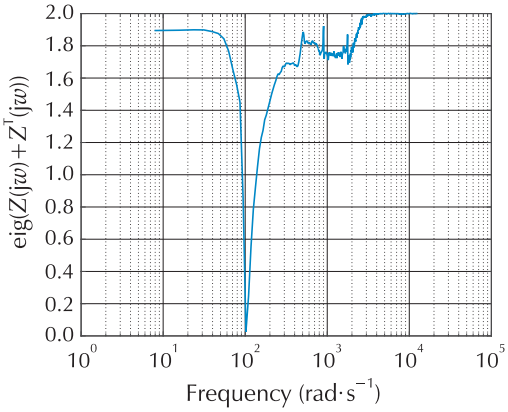

Fig. 9 Minimum eigenvalue of $Z(s)$ (for $K_{\min_1}$, $K_{\max_1}$) versus frequency for the $\mathscr{U}_3$ and gain-decreasing $\mathscr{U}_1$ NDC.

6.6.2 Sector 2

Sector 2 is $K_{\min_2} = \text{diag}\{0.5, 0.0275, 0.9999\}$, $K_{\max_2} = I$. The (2, 2) and (3, 3) elements are selected to determine the sector for $A(u)$ (i.e., the (1, 1) elements) for which the system is absolutely stable over the range of the actuator ±0.2 V (note that saturation B_{11} is subsumed by sector [0.0275 1] over domain [−0.2 0.2] and B_3 is unit gain over the range of the actuator). Fig. 10 shows the characteristic loci for $K_{\min_2} T_{\text{eq}}(s)$; there are no encirclements of the critical point (−1 + j0) and as the open loop system is stable, $M(s)$ is stable by the Generalized Nyquist Theorem (condition (2) in Section 5). Fig. 11 shows the minimum eigenvalues of $Z(\text{j}\omega) + Z^{\text{T}}(-\text{j}\omega)$ as a function of frequency, showing that conditions (2) and (3) for strict positive reality in Section 5 are satisfied (all poles of $Z(s)$ have negative real parts, condition (1)), thus condition (3) of the Circle Criterion is satisfied and the system is absolutely stable over this sector (the system is stable for any nonlinearity $A(u)$ in sector [0.5 1] over the range of the actuator).

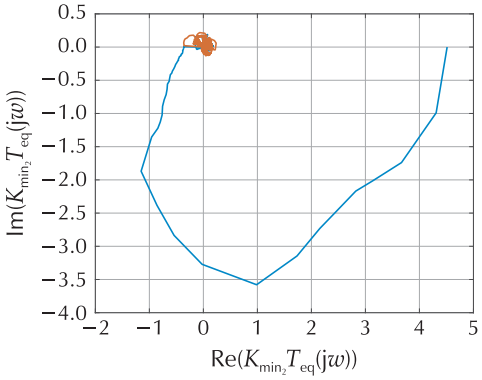

Fig. 10 Characteristic loci $K_{\min_2} T_{\text{eq}}(s)$ for the $\mathscr{U}_3$ and gain-decreasing $\mathscr{U}_1$ NDC.

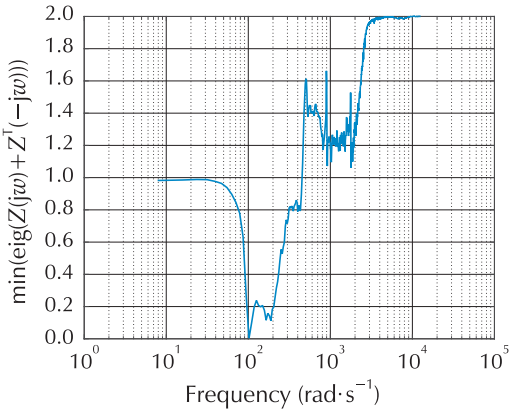

Fig. 11 Minimum eigenvalue of Z(s) (for $K_{\min_2}$, $K_{\max_2}$) versus frequency for the $\mathscr{U}_3$ and gain-decreasing $\mathscr{U}_1$ NDC.

6.7 PLRQC

PLRQC is applied to the parallel mechanism. Four $\mathscr{U}_1$ plant responses ($P_j(s)$, $j = 1, 2, 3, 4$) of diminishing modulus at low frequency (i.e., over the control bandwidth, the modulus of $P_1(s)$ is greater than $P_2(s)$, etc.) are modeled. Note that experimentally acquired frequency response data can be used as a surrogate for rational functions fitted to the data. Threshold values for the nonlinear functions described in equation (13) are selected using engineering judgment, and linear systems are found using equation (12). The pole-zero-gain representations of the PLR linear systems are summarized in Tables 6–9. $N_{14q}(s)$ works in concert with the other three systems of the PLR to reduce the loop transmission in very low $\mathscr{U}_1$. $B_{1i}(u)$ are saturations with limits 0.014, 0.012, 0.005, 0.003. $B_3(u)$ is identical to the GDNDC (saturation with limit 0.2).

Table 6 PZK model of the $N_{11}(s)$.

K	s_z	s_p
-1.2130×10^3	-1.3195×10^3	-2.5133×10^3
	$(-0.2827 \pm 0.8991\text{i}) \times 10^3$	$(-0.3204 \pm 1.0189\text{i}) \times 10^3$
	-0.5655×10^3	$(-0.5655 \pm 0.2739\text{i}) \times 10^3$
	-0.2513×10^3	-0.2827×10^3
	-0.0063×10^3	-0.0094×10^3

Table 7 PZK model of the $N_{12}(s)$.

K	s_z	s_p
-2.6932×10^6	$(-2.0735 \pm 6.5932\text{i}) \times 10^2$	$(-0.8482 \pm 2.6972\text{i}) \times 10^3$
	$(-1.0210 \pm 3.9544\text{i}) \times 10^2$	$(-0.2042 \pm 0.7909\text{i}) \times 10^3$
	-2.8274×10^2	$(-0.0543 \pm 0.4491\text{i}) \times 10^3$
		-0.1885×10^3

Table 8 PZK model of the $N_{13}(s)$.

K	s_z	s_p
-9.5287×10^8	$(-0.5278 \pm 4.3664\mathrm{i}) \times 10^2$	-5.0265×10^3 -5.0265×10^3 $(-0.0236 \pm 0.4706\mathrm{i}) \times 10^3$ -0.3142×10^3

Table 9 PZK model of the $N_{14_q}(s)$.

K	s_z	s_p
2.6809×10^{13}	$(-0.4060 \pm 4.6589\mathrm{i}) \times 10^2$ $(-0.5967 \pm 4.4364\mathrm{i}) \times 10^2$ $(-1.9407 \pm 3.2447\mathrm{i}) \times 10^2$ -2.9857×10^2 -1.9813×10^2 $(-0.1521 \pm 0.9540\mathrm{i}) \times 10^2$ $(-0.4124 \pm 0.5607\mathrm{i}) \times 10^2$	-1.8850×10^4 -1.8850×10^4 -1.8849×10^4 $(-0.0302 \pm 0.0402\mathrm{i}) \times 10^4$ $(-0.0047 \pm 0.0469\mathrm{i}) \times 10^4$ $(-0.0054 \pm 0.0449\mathrm{i}) \times 10^4$ -0.0377×10^4 -0.0188×10^4 $(-0.0013 \pm 0.0062\mathrm{i}) \times 10^4$ $(-0.0034 \pm 0.0025\mathrm{i}) \times 10^4$

6.7.1 Sector 3

Sector matrices are 6×6 diagonal matrices. The $(1,1)$ elements bound a sector for nonlinearity $A(u)$, the $(2,2)$–$(5,5)$ elements bound sectors for the four B_{1i} NDC nonlinearities, and the $(6,6)$ elements bound the B_3 nonlinearity. Sector 3 is $K_{\min_3} = \mathrm{diag}\{0, 0.999, 0.95, 0.9, 0.84, 0.999\}$, $K_{\max_3} = \mathrm{diag}\{0.33, 1, 1, 1, 1, 1\}$. This sector is selected to determine stability for small signal nonlinear responses of $A(u)$ (for this case, sector [0 0.33]). Fig. 12 shows the characteristic loci for $K_{\min_3} T_{\mathrm{eq}}(s)$; there are no encirclements of the critical point $(-1 + \mathrm{j}0)$ and as the open loop system is stable, $M(s)$ is stable by the Generalized Nyquist Theorem (condition (2) in Section 5.

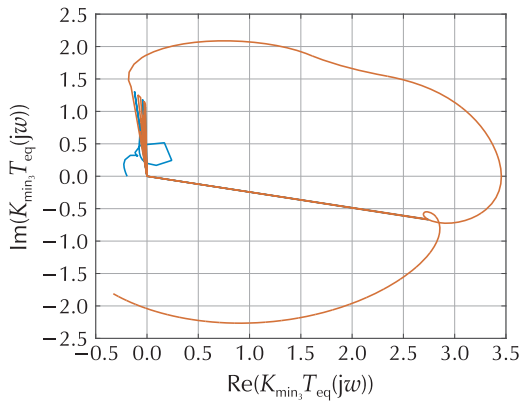

Fig. 12 Characteristic loci $K_{\min_3} T_{\mathrm{eq}}(s)$ for the $\mathscr{U}_3$ and PLRQC.

Fig. 13 shows the minimum eigenvalues of $Z(\mathrm{j}\omega) + Z^{\mathrm{T}}(-\mathrm{j}\omega)$ as a function of frequency, showing that conditions (2) and (3) for strict positive reality in Section 5 are satisfied (all poles of $Z(s)$ have negative real parts, condition (1)), thus condition (3) of the Circle Criterion is satisfied and the system is absolutely stable over this sector.

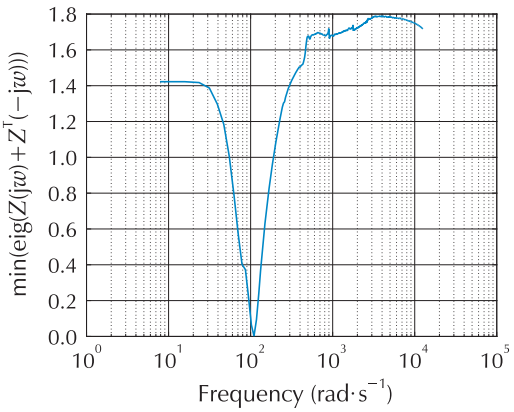

Fig. 13 Minimum eigenvalue of Z(s) (for $K_{\min_3}$, $K_{\max_3}$) versus frequency for the $\mathscr{U}_3$ and PLRQC.

Recall the $B_{14}(u)$ is the saturation with limit 0.003, so the lower sector limit of 0.84 intersects this at $u = \pm 0.00357$, and thus this is the domain for which the system is absolutely stable for this sector (approximately 2 percent of the actuator range).

6.8 Effect of quiescent compensation on response

Figs. 14 and 15 show sensor signal spectra when the system is driven by Levels 1 and 2 disturbances. Each plot shows spectra for three closed-loop responses: a gain-increasing NDC ($m=1$ in equation (12)), PLR ($m=4$ in equation (12)), and PLRQC ($m=5$ in equation (12)). Performance comparisons of gain-decreasing and gain-increasing NDC schemes are presented in [36]. The effect of quiescent compensation is evident in Fig. 14, where reduced regenerative response is seen in the neighborhood of crossover viz-a-viz GINDC or PLR with the trade-off of less feedback applied over the functional bandwidth. This effect is reduced as the disturbance power is increased as evident in Fig. 15.

In Fig. 14, the superior performance over the 10 Hz (63 rad/s) functional bandwidth of the gain-increasing NDC designs (GI and PLR) in $\mathscr{U}_1$ is expected, as the NDC reestablishes the large Nyquist-stable loop gain in this condition. The sharp peaks of regenerative response in the GINDC data due to the positive feedback in the octave 50–100 Hz are a consequence of the inadequacy of the single-path gain-reestablishment approach in $\mathscr{U}_1$. The peaks in the PLR response are substantially lower than those of GINDC while delivering the same performance over the functional bandwidth. An application of quiescent compensation further reduces the effect of positive feedback around crossover frequency, but also reduces performance over the functional bandwidth. With an increase in the disturbance power, system performance using quiescent compensation is greater than using GINDC or PLR, as demonstrated in Fig. 15. PLRQC response shows better reduction of the regenerative behavior and larger amount of feedback applied over the functional bandwidth than other NDC designs.

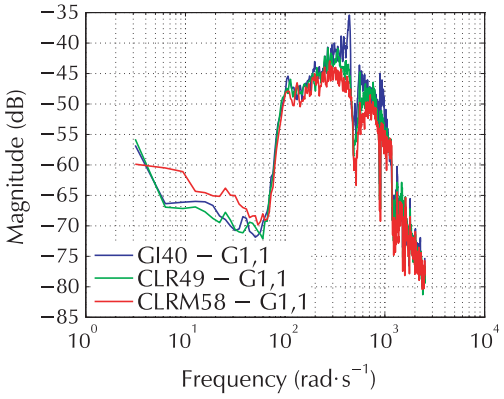

Fig. 14 Level 1 disturbance responses. The blue function (GI40) is the response of the system with gain increasing NDC. The green (CLR49): PLR. The red (CLRM58): PLRQC.

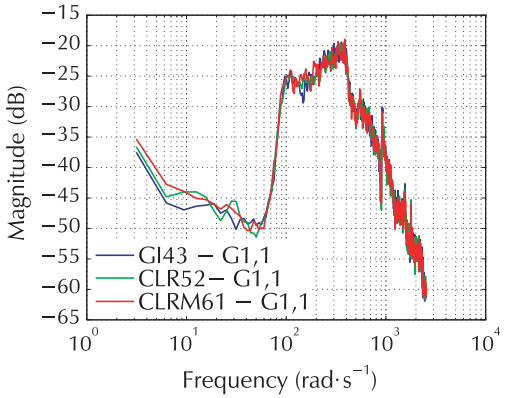

Fig. 15 Level 2 disturbance responses. The blue function (GI43) is the response of the system with gain increasing NDC. The green (CLR52): PLR. The red (CLRM61): PLRQC.

7 Conclusions

A method to apply multiple nonlinear dynamic compensators combined with linear Nyquist-stable compensators for large-feedback/high-performance applications on systems with imperfect and limited actuators is presented. Large feedback linear controllers are very sensitive to variations in loop transmission and may oscillate when applied to systems with these actuators. The improved NDC approach maintains stability in actuator saturation and eliminates oscillation due to the influence of nonlinearities at low amplitude by effecting changes in the loop gain. The efficacy of the approach is shown with closed-loop data and multivariable absolute stability analysis on a voice-coil actuator used in a vibration suppression system.

References

[1] S. Tarbouriech, M. Turner. Anti-windup design: An overview of some recent advances and open problems. *IET Control Theory and Applications*, 2009, 3(1): 1 – 19.

[2] S. Galeani, S. Tarbouriech, M. Turner, et al. A tutorial on modern anti-windup design. *Proceedings of the European Control Conference*. Piscataway: IEEE, 2009: 306 – 323.

[3] S. Miyamoto, G. Vinnicombe. Robust control of plants with saturation nonlinearity based on coprime factor representations. *Proceedings of the 35th IEEE Conference on Decision and Control*, Piscataway: IEEE, 1996: 2838 – 2840.

[4] P. F. Weston, I. Postlethwaite. Linear conditioning for systems containing saturating actuators. *Automatica*, 2000, 36(9): 1347 – 1354.

[5] G. Grimm, I. Postlethwaite, A. R. Teel, et al. Linear matrix inequalities for full and reduced order anti-windup synthesis. *Proceedings of the American Control Conference*, Piscataway: IEEE, 2001: 4134 – 4139.

[6] M. Bruckner, S. Galeani, L. Del Re. An alternative solution to the weakened anti-windup problem for LFT perturbed plants. *IFAC Proceedings Volumes*, 2011, 44(1): 13420 – 13425.

[7] A. Marcos, M. C. Turner, I. Postlethwaite. An architecture for design and analysis of high-performance robust antiwindup compensators. *IEEE Transactions on Automatic Control*, 2007, 52(9): 1672 – 1679.

[8] J. J. E. Slotine, W. Li. *Applied Nonlinear Control*. Englewood Cliffs: Prentice Hall, 1991.

[9] H. K. Khalil. *Noninear Systems*. Upper Saddle River: Prentice Hall, 1996.

[10] J. C. A. De Bruin, A. Doris, N. van de Wouw, et al. Control of mechanical motion systems with non-collocation of actuation and friction: A Popov criterion approach for input-to-state stability and set-valued nonlinearities. *Automatica*, 2009, 45(2): 405 – 415.

[11] B. Lurie, P. Enright. *Classical Feedback Control: with MATLAB*. Boca Raton: CRC Press, 2000.

[12] G. W. Neat, J. F. O'Brien. Micro-precision interferometer: Fringe tracker control system. *Advances in the Astronautical Sciences*, 1996, 92(5): 501 – 516.

[13] J. F. O'Brien. Multi-path nonlinear dynamic compensation for rudder roll stabilization. *Control Engineering Practice*, 2009, 17(12): 1405 – 1414.

[14] J. O'Brien. *Frequency-domain Control Design for High Performance Systems*. London: The Institution of Engineering and Technology, 2012.

[15] M. Heertjes, F. Cremers, M. Rieck, et al. Nonlinear control of optical storage drives with improved shock performance. *Control Engineering Practice*, 2005, 13(10): 1295 – 1305.

[16] J. F. O'Brien. Trends in region 3 control system performance control system performance as wind turbine size increases. *Journal of Automatic Control and System Engineering*, 2012, 12(1): 45 – 55.

[17] Y. V. O'Brien, J. F. O'Brien. Stability analysis of a single-input/two-output, variable loop transmission system for wind turbine control. *Conference on Science of Making Torque from Wind (TORQUE)*. Bristol: IOP Publishing, 2016: DOI 10.1088/1742-6596/753/5/052028.

[18] Y. O'Brien, J. O'Brien. Variable, large feedback wind turbine control synthesis with limited plant information. *The 2nd International Conference on Future Technologies in Wind Energy*, London: WindEEE Research Institute, 2015: 105 – 106.

[19] C. C. De Wit, H. Olsson, K. J. Astrom, et al. A new model for control of systems with friction. *IEEE Transactions on Automatic Control*, 1995, 40(3): 419 – 425.

[20] N. E. Ehrich. *An Investigation of Control Strategies for Friction Compensation*. Fort Belvoir: Defense Technical Information Center, 1991.

[21] H. J. Hunink, M. Steinbuch. *Modelling, Analysis and Control of Mechanical Servo-systems with Friction A Survey of Literature*. Amsterdam: Phillips Electronics N. V., 1994.

[22] H. Olsson, K. J. Astrom, C. C. De Wit, et al. Friction models and friction compensation. *Europian Journal of Control*, 1998, 4(3): 176 – 195.

[23] P. J. Blau. *Friction Science and Technology: from Concepts to Applications*. Boca Raton: CRC Press, 2008.

[24] J. Tou, P. M. Schultheiss. Static and sliding friction in feedback systems. *Journal of Applied Physics*, 1953, 24(9): 1210 – 1217.

[25] B. Armstrong, B. Amin. PID control in the presence of static friction: A comparison of algebraic and describing function analysis. *Automatica*, 1996, 32(5): 679 – 692.

[26] S. I. Cho, I. J. Ha. A learning approach to tracking in mechanical systems with friction. *IEEE Transactions on Automatic Control*, 2000, 45(1): 111 – 116.

[27] J. H. Ryu, J. Song, D. S. Kwon. A nonlinear friction compensation method using adaptive control and its practical application to an in-parallel actuated 6-DOF manipulator. *Control Engineering Practice*, 2001, 9(2): 159 – 167.

[28] P. Vedagarbha, D. M. Dawson, M. Feemster. Tracking control of mechanical systems in the presence of nonlinear dynamic friction effects. *IEEE Transactions on Control Systems Technology*, 1999, 7(4): 446 – 456.

[29] T. H. Kim, I. J. Ha. Time-optimal control of a single-DOF mechanical system with friction. *IEEE Transactions on Automatic Control*, 2001, 46(5): 751 – 755.

[30] L. R. Ray, A. Ramasubramanian, J. Townsend. Adaptive friction compensation using extended Kalman¨CBucy filter friction estimation. *Control Engineering Practice*, 2001, 9(2): 169 – 179.

[31] Y. Yao, X. Huo, K. Zheng, et al. Nonsmooth control design of mechanical systems with friction in the sense of Filippov. *Proceedings of the 8th World Congress on Intelligent Control and Automation*, Piscataway: IEEE, 2010: 3622 – 3626.

[32] T. Nakakuki, K. Tamura. Control design of nonlinear mechanical systems with friction. *Proceedings of the 43rd IEEE Conference on Decision and Control*, Piscataway: IEEE, 2004: 2966 – 2971.

[33] V. Lampaert, J. Swevers, F. Al-Bender. Modification of the Leuven integrated friction model structure. *IEEE Transactions on Automatic Control*, 2002, 47(4): 683 – 687.

[34] B. Potsaid, J. T. Y. Wen, M. Unrath, et al. High performance motion tracking control for electronic manufacturing. *Journal of Dynamic Systems, Measurement, and Control*, 2007, 129(6): 767 – 776.

[35] C. L. Mock, Z. T. Hamilton, D. Carruthers, et al. Nonlinear compensation for high performance feedback systems with actuator imperfections. *Proceedings of the ASME Dynamic Systems and Control Conference*, New York: ASME, 2013: DOI 10.1115/DSCC2013-3741.

[36] J. F. O'Brien, D. J. Carruthers. Nonlinear dynamic compensation for large-feedback control of a servomechanism with multiple nonlinearities. *Control Engineering Practice*, 2013, 21(11): 1531 – 1541.

[37] H. W. Bode. Relations between attenuation and phase in feedback amplifier design. *Bell Labs Technical Journal*, 1940, 19(3): 421 – 454.

[38] D. Carruthers, J. O'Brien. Two degree-of-freedom parallel mechanisms for high bandwidth vibration suppression and tracking. *Proceedings of the SPIE Symposium on Smart Structures and Materials*, Bellingham: SPIE, 2011: DOI 10.1117/12.880064.

[39] J. M. Maciejowski. *Multivariable Feedback Design*. Wokingham: Addison-Wesley, 1989.

[40] D. J. Carruthers, J. F. O'Brien, J. E. McInroy, et al. Development of a voice coil-actuated limited-degree-of-freedom parallel mechanism for vibration suppression. *Proceedings of the Institution of Mechanical Engineers, Part I: Journal of Systems and Control Engineering*, 2009, 223(1): 85 – 94.

[41] P. J. Nelson, D. J. Carruthers, J. F. O'Brien, et al. Design and control of a two-arm parallel mechanism using revolute and prismatic actuators. *Proceedings of the IASTED Technology Conferences*, Calgary: ACTA Press, 2010: 706025 – 706045.

[42] J. A. Parkins, J. F. O'Brien. A modified command feedforward tracking control system applied to the PRRR-RR parallel mechanism. *Proceedings of the Active and Passive Smart Structures and Integrated Systems*, Bellingham: SPIE, 2012: DOI 10.1117/12.917513.

[43] J. E. McInroy, J. F. O'Brien, A. A. Allais. Designing micromanipulation systems for decoupled dynamics and control. *IEEE/ASME Transactions on Mechatronics*, 2015, 20(2): 553 – 563.

[44] A. A. Allais, J. E. McInroy, J. F. O'Brien. A new class of locally decoupled Gough-Stewart platform manipulators. *Proceedings of the IEEE/RSJ International conference on Intelligent Robots and Systems*, Piscataway: IEEE, 2012: 1561 – 1566.

Yelena V. O'BRIEN received the B.Sc. degree from University of Maryland, College Park, in 1997, and M.Sc. degree from Rensselaer Polytechnic Institute in 1999. She worked as a gas/steam turbine control requisition engineer at General Electric Power Systems until 2002 and as a senior engineer at General Dynamics Land Systems until 2003. She is currently a Ph.D. candidate at the University of Wyoming. Her research interest is nonlinear dynamic compensation. E-mail: obrieny@uwyo.edu.

John F. O'BRIEN received the Ph.D. degree from Rensselaer Polytechnic Institute in 2001. He is an Associate Professor of Electrical and Computer Engineering at the University of Wyoming. He was a Member of Technical Staff at NASA's Jet Propulsion Laboratory in the 1990s where he researched control applied to active space structures. His current research interest is high performance control with nonlinear compensation. E-mail: obrienj@uwyo.edu.